

Direct Wireless Link to Out-of-Range Node With Assistance of Surrounding Nodes

Hiroya Tanaka¹, Senior Member, IEEE, Shintaro Hiraoka², Student Member, IEEE,
Shintaro Arai³, Member, IEEE, Takaya Yamazato⁴, Senior Member, IEEE,
and Yukihiro Tadokoro⁵, Senior Member, IEEE

Abstract—We propose a method that establishes a direct wireless link from a transmission source to an out-of-range destination with the assistance of the surrounding communication nodes. In this method, a weak (subthreshold) signal is amplified by utilizing the interference signals transmitted from the surrounding communication nodes. To evaluate the amplification gain, we study the mutual information in a multipath fading channel. As a result, we reveal that the mutual information is enhanced owing to the interference signals, and the proposed method enlarges the radio coverage area of the source node. To understand the enhancement mechanism, we introduce a toy model of the propagation channel and discuss the role of the interference signals. We find that the interference signals allow the subthreshold signals into the detectable region in the signal space. Moreover, the mutual information is maximized at the optimal power of the interference signals. In addition, a detailed discussion of the channel capacity shows that there exists an optimal *a priori* probability of symbol transmission.

Index Terms—Channel capacity, noise-aided enhancement, stochastic resonance, subthreshold signal detection.

I. INTRODUCTION

IN WIRELESS communications, the enhancement of radio coverage is of fundamental interest because it is a key factor that determines the quality of service. Considerable effort has been devoted to the enhancement of radio coverage using relay networks [1], [2] and/or multiantenna technologies [3]. In this study, we offer another solution to this fundamental problem that exploits interference signals.

It has been reported that the detectability of weak (subthreshold) signals is enhanced by noise via the transduction of nonlinear elements [4], [5]. This phenomenon, called stochastic resonance (SR), has been thoroughly discussed in the context of

nonlinear physics [4]–[14]. In the last two decades, SR has been applied to several systems in various fields of engineering, e.g., optics [15], [16], imaging [17]–[19], and computing [20]–[22]. Because the received signal is often attenuated and weakened in wireless communications, many researchers have examined the use of SR to improve communication performance; in cognitive radio, weak signals have been successfully detected with SR-based sensing schemes [23]–[26]. A stochastic resonator was proposed to improve the bit-error rate for binary data transmission with a pulse-amplitude-modulated signal [27]. Amazingly, multilevel pulse-amplitude-modulated signals were successfully estimated at the receiver with an amplitude resolution of only one bit [28]. The essence of these enhancements is the modulation of the probability density [5], [19], [29]; owing to the nonlinear behavior with noise, the probability density for correct detection is changed to one that improves performance.

Traditional communication systems generally attempt to suppress interference signals to avoid erroneous detection. However, along with SR, such bothersome signals may aid in correct detection by amplifying weak signals; in a multipath fading channel, the behavior of such signals can be treated as stochastic like noise; hence, an enhancement effect should be obtained. In fact, the exploitation of such signals can enhance the channel capacity in polarization diversity reception [30]. This is because the detection limit is stochastically depressed owing to the change in the probability density of the received symbols at the detector input.

In this paper, we analytically explore the possibility of enhancing radio coverage by exploiting the stochastic behavior of interference signals. To investigate this, we focus on the fundamental multipath fading scenario of Rician fading and introduce a decision region for a signal originating from an out-of-range node. As modulation schemes, on–off keying (OOK) and M -ary phase-shift keying (M -PSK) are considered, and numerical results focusing on the mutual information show that even the signals from out-of-range nodes can be successfully detected. As a result, the coverage area can be enlarged with an alternative approach that is inherently different from conventional methods such as relay networks and multiantenna technologies [1]–[3].

For better comprehension, an intuitive understanding of the enhancement is provided with a *toy model* in Section IV. A theoretical analysis focusing on the probability density function (PDF) of the received symbol gives us the enhancement mechanism; specifically, the interference signals widen the PDF

Manuscript received March 25, 2019; revised June 28, 2019 and July 31, 2019; accepted August 4, 2019. Date of publication September 12, 2019; date of current version November 12, 2019. This work was supported in part by JSPS KAKENHI under Grant 18K04157. The review of this article was coordinated by Prof. R. Dinis. (Corresponding author: Hiroya Tanaka.)

H. Tanaka and Y. Tadokoro are with Toyota Central R&D Laboratories, Inc., Aichi 480-1192, Japan (e-mail: tanak@mosk.tytlabs.co.jp; y.tadokoro@ieee.org).

S. Hiraoka was with the Nagoya University, Nagoya 464-8603, Japan. He is now with, Chūkyō Television Broadcasting Co., Ltd., Nagoya 453-8704, Japan (e-mail: hiraoka@katayama.nuee.nagoya-u.ac.jp).

S. Arai is with the Okayama University of Science, Okayama 700-0005, Japan (e-mail: arai@ee.ous.ac.jp).

T. Yamazato is with the Nagoya University, Nagoya 464-8603, Japan (e-mail: yamazato@nagoya-u.jp).

Digital Object Identifier 10.1109/TVT.2019.2934502

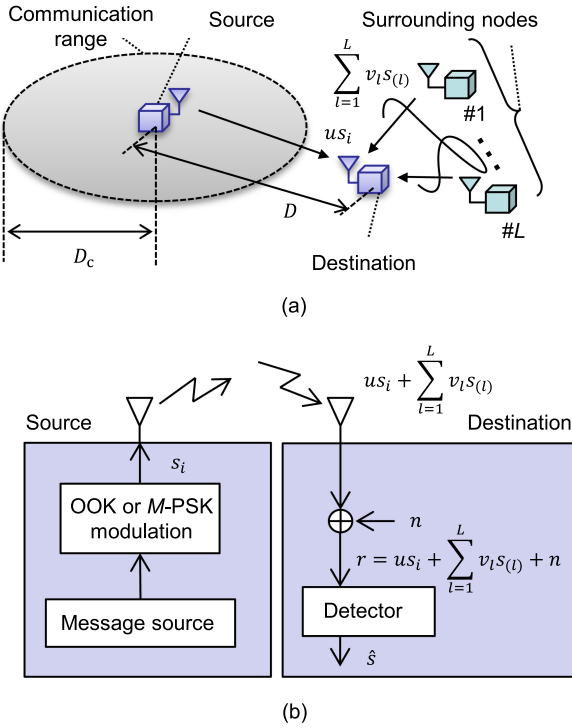


Fig. 1. (a) Schematic of system model. (b) System configuration of the source and destination.

so that a signal originating from an out-of-range node could often exceed the detection limit. Indeed, previous work [30] has addressed this point; however, it is found that interference signals that are too strong deteriorate the phase, which results in a detection error. In this sense, there exist interference signals with an optimal variance that provide correct detection. Through a theoretical discussion of the channel capacity, it is revealed that certain signal points cannot transfer information; the channel capacity can be obtained even without the symbols that belong to these points. This finding should be valuable for the design of modulation schemes.

The paper is organized as follows. In Section II, we present the proposed system and general propagation model that are the focus of this work. In Section III, we numerically analyze the performance of the proposed method in terms of the mutual information. To understand the enhancement mechanism, we introduce a *toy model* and discuss the stochastic behavior of the proposed method in Section IV. In Section V, we derive the performance limit, i.e., the channel capacity, of the proposed method. Finally, we conclude with some final remarks in Section VI.

II. PROPOSED METHOD

Fig. 1(a) shows a system model of a single communication link between the source and destination nodes considered in this work. The source and destination are separated by the distance D , and the destination is surrounded by L nodes (surrounding nodes). The communication range of the source is within the shaded circle of radius D_c . Here, we focus on the critical situation where the destination and all of the surrounding nodes

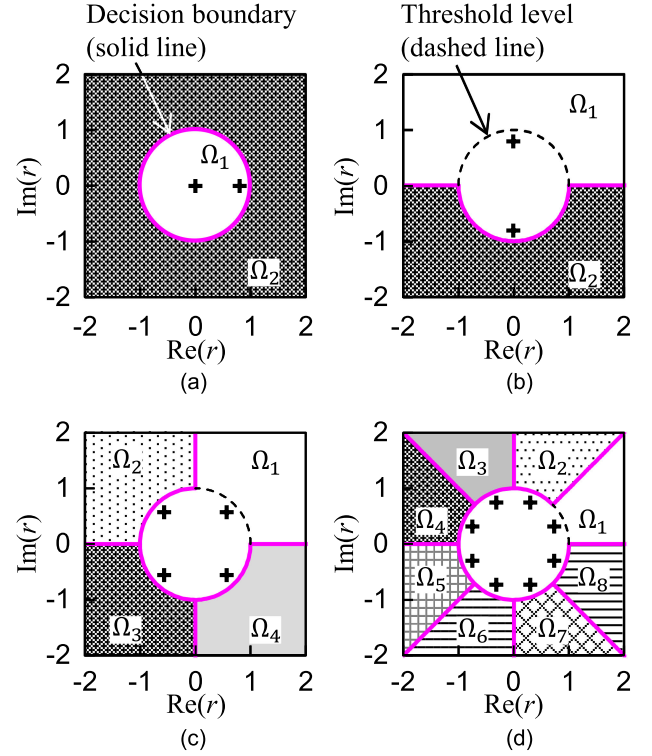


Fig. 2. Signal space diagrams and decision regions for (a) OOK, (b) 2-PSK, (c) 4-PSK, and (d) 8-PSK modulation at $\xi = 1$. Crosses represent the message points s_i , which are plotted by setting the parameters as $|us_i| = 0.8$ and $\sum_{l=1}^L v_l s_l = n = 0$ in (3).

are located outside the communication range of the source. Because $D > D_c$, the signal transmitted from the source is not detectable at the destination. Moreover, no surrounding nodes can help transmit the message from the source to the destination because relaying techniques are inapplicable. This situation is often encountered in multipath fading environments.

To overcome such a severe situation, we propose a method that enlarges the coverage range of the source using the signals transmitted by the surrounding nodes, which is based on the concept of SR. Fig. 1(b) presents the system configuration of the source and destination nodes. A message is transmitted with M -PSK and OOK modulation. An analytical expression for the transmitted symbol is provided with the equivalent low-pass signal [31]; for M -PSK, the transmitted symbol s_i is given as

$$s_i = A e^{j \frac{(2i-1)\pi}{M}} \quad (1)$$

according to the selected message m_i , where $i \in \mathbb{N}$ is the index of the messages, which are $i = \{1, 2\}$ for OOK and 2-PSK, $i = \{1, \dots, 4\}$ for 4-PSK, and $i = \{1, \dots, 8\}$ for 8-PSK. The variable M is the number of message points in the signal space, which takes values of 2, 2, 4, and 8 for OOK, 2-PSK, 4-PSK, and 8-PSK, respectively. The parameter $A \in \mathbb{R}$ quantifies the amplitude of the transmitted symbol. For OOK, a transmitted symbol has the form

$$s_i = A(i-1), \quad (2)$$

where $i = 1$ and 2. Fig. 2 shows the signal space diagrams for OOK and M -PSK modulation, where crosses represent the message points.

Because the surrounding nodes also transmit their symbols $s_{(l)}$, the symbol r received at the destination is expressed as

$$\begin{aligned} r &= us_i + \sum_{l=1}^L v_l s_{(l)} + n \\ &\equiv ae^{j\phi}, \end{aligned} \quad (3)$$

where u is the complex-valued channel response for the transmitted symbol s_i , v_l is the complex-valued channel response for the symbol transmitted from the l -th surrounding node, and n is the noise. The variables $a \in \mathbb{R}$ and $\phi \in \mathbb{R}$ represent the amplitude and phase of the received symbol, respectively. If the multipath fading channel u is expressed as the sum of the channel responses for each propagation path, $u = \sum_{g=1}^{N_u} \nu_g e^{j\theta_g}$, where ν_g and θ_g are the attenuation factor and phase shift on the g -th path, respectively, and N_u is the number of paths. Similarly, for the channel of the l -th surrounding node, $v_l = \sum_{g=1}^{N_{v_l}} \chi_{lg} e^{j\psi_{lg}}$, where χ_{lg} and ψ_{lg} are the attenuation factor and phase shift on the g -th path, respectively, and N_{v_l} is the number of paths. Note that the parameters ν_g , θ_g , χ_{lg} , and ψ_{lg} are random variables owing to the statistical behavior of the multipath channel. Moreover, because the signal from the source cannot reach both the destination and surrounding nodes, the surrounding nodes do not know the symbols transmitted from the source, and they cannot relay the symbol s_i . Hence, the symbol transmitted from the surrounding nodes, $s_{(l)}$, is independent of that from the source, s_i , for any index l .

In the scenario in Fig. 1(a), the transmitted symbol s_i is greatly attenuated owing to the term u ; thus, detection errors often occur. However, following the concept of SR, the interference symbol $\sum v_l s_{(l)}$ should amplify the transmitted symbol us_i ; when N_{v_l} is sufficiently large, the interference symbol behaves as noise that plays a key role in the enhancement by SR.

To achieve such amplification, nonlinear signal processing, i.e., hard decision decoding, is introduced at the destination. More specifically, the received symbol r is detected in accordance with the decision region to which the received symbol belongs. For OOK, the decision region Ω_i is

$$\Omega_1 = \{a : a \leq \xi\}, \quad (4a)$$

$$\Omega_2 = \{a : a > \xi\} = \bar{\Omega}_1, \quad (4b)$$

where ξ is the threshold level of the amplitude. The detected symbol \hat{s} is then obtained as

$$\hat{s} = s_i \quad \text{if } r \in \Omega_i. \quad (5)$$

For M -PSK, the received symbol is similarly detected following the decision region:

$$\Omega_1 = \{(a, \phi) : a \leq \xi\} \cup \left\{ (a, \phi) : a > \xi, |\phi| < \frac{\pi}{M} \right\}, \quad (6a)$$

$$\Omega_{i \neq 1} = \left\{ (a, \phi) : a > \xi, \frac{(2i-3)\pi}{M} \leq \phi < \frac{(2i-1)\pi}{M} \right\}. \quad (6b)$$

Note that the threshold level ξ is not tunable because this level is determined by the implementation of the RF circuit. In this paper, we discuss communication with an out-of-range node for a given threshold level ξ .

The decision regions are illustrated in Fig. 2. The decision boundaries in (4a), (4b), (6a), and (6b) are simply set to ensure that the following rules are met: for OOK, r lies in Ω_2 if r is larger than the threshold levels, and for M -PSK, r lies in Ω_i if the distance $|r - s_k|$ is minimized for $k = i$. Since the threshold ξ is the detection limit at the destination, the threshold amplitude is expressed by a circle of radius ξ in the signal space. The destination cannot detect the subthreshold symbols, which exist inside the circle (i.e., $a < \xi$). Thus, the symbols transmitted from the source cannot be detected on the basis of these received subthreshold symbols. For simplicity, the subthreshold symbol is discriminated as being in region Ω_1 regardless of the transmitted symbol. In OOK, because the symbol $s_1 = 0$ should have a small amplitude, the subthreshold symbol should be detected as s_1 . In M -PSK, the subthreshold symbol is tentatively detected as the symbol s_1 .

Again, even in the severe situation $a < \xi$, the transmitted symbol s_i should be successfully detected via the help of the interference symbol $\sum_{l=1}^L v_l s_{(l)}$ and the hard decision decoder. The interference symbol provides significant amplification, which is maximized at a certain interference level. We discuss the detailed mechanism of amplification in Section IV.

Our fundamental study explores the possibility of communication among the out-of-range nodes with the help of the interference signals. For simplicity, we focus on a general radio propagation model, i.e., a Rician fading channel, and the enhancement effect is analytically evaluated with the theoretical limit of the channel capacity. Since this fading model is used in the evaluation of a wide range of wireless communication channels, including relay networks [32], [33], fifth generation (5G) [34] and developing 802.11 systems [35], our results should be effective in many scenarios of wireless communication, and it is expected that the proposed method will provide further improvements in long-range communication. As a side note, the parameters are listed in Table I.

III. PERFORMANCE RESULTS

In this section, we show that the interference symbol enhances the mutual information. We first derive the PDF of the received symbol in a multipath fading channel. Next, we numerically calculate the mutual information. Throughout the analysis, we demonstrate that the interference symbol allows us to enlarge the communication range of the source.

A. Probability Density of the Received Symbol

We now derive the PDF of the received symbol r in a common propagation model, where the numbers of paths (N_u and N_{v_l}) are sufficiently large and the channel responses (u and v_l) are assumed to be independent. Thus, the communication channel in Fig. 1 is described as a Rician fading channel; the term u is assigned to the dominant path $\nu_{g_d} e^{j\theta_{g_d}} s_i$, and the residual multipath component $\sum_{g \neq g_d} \nu_g e^{j\theta_g} s_i$, where $g = g_d$ corresponds

TABLE I
SYMBOL DEFINITIONS

Symbols	Description
D	Distance between the source and destination nodes
D_c	Communication range of the source
M	Number of message points
L	Number of surrounding nodes
A	Amplitude of the transmitted symbol
s_i and \hat{s}	Transmitted and detected symbols
i and k	Indexes of the messages
u and v_l	Complex-valued channel responses for s_i and $s_{(l)}$
l	Index of the interference symbols
$s_{(l)}$	Symbol transmitted from the l -th surrounding node
r	Symbol received at the destination
a and ϕ	Amplitude and phase of the received symbol r
ν_g and χ_{lg}	Attenuation factors of the g -th path for s_i and $s_{(l)}$
θ_g and ψ_{lg}	Phase shifts of the g -th path for s_i and $s_{(l)}$
N_u and N_{v_l}	Numbers of paths for s_i and $s_{(l)}$
n	Noise at the destination
Ω_i	Decision region
g_d	Index of the dominant path
ξ	Threshold level
ρ	Amplitude of the dominant path
σ^2	Variance of $\text{Re}(r)$ and $\text{Im}(r)$
σ_u^2	Variance of $\text{Re}\left(\sum_{k \neq k_d} \nu_k e^{j\theta_k}\right)$ and $\text{Im}\left(\sum_{k \neq k_d} \nu_k e^{j\theta_k}\right)$
σ_v^2	Variance of $\text{Re}\left(\sum_l v_l s_{(l)}\right)$ and $\text{Im}\left(\sum_l v_l s_{(l)}\right)$
σ_n^2	Variance of $\text{Re}(n)$ and $\text{Im}(n)$
κ	Rician K-factor for the channel response u
$p_{\sigma^2}(a, \phi s_i)$	Joint PDF of the received symbol r
α_i	<i>A priori</i> probability $P[s_i]$
$I(S; \hat{S})$	Mutual information
S	Set of transmitted symbols $\{s_1, \dots, s_M\}$
\hat{S}	Set of detected symbols $\{\hat{s}_1, \dots, \hat{s}_M\}$
P_{ki}	Channel transition probability $P[\hat{s} = s_k s_i]$

to the dominant path. Equation (3) is now rewritten as

$$r = \rho s_i + \sum_{g=1, g \neq g_d}^{N_u} \nu_g e^{j\theta_g} s_i + \sum_{l=1}^L v_l s_{(l)} + n, \quad (7)$$

where $\rho \equiv \nu_{g_d}$ and, without loss of generality, $\theta_{g_d} = 0$.

In the Rician fading channel, the in-phase and quadrature components of the received symbol r have Gaussian distributions. The mean and variance, which are the key variables for characterizing the PDF, are given as

$$E[\text{Re}(r)] = \rho \text{Re}(s_i), \quad (8a)$$

$$E[\text{Im}(r)] = \rho \text{Im}(s_i), \quad (8b)$$

$$\text{Var}[\text{Re}(r)] = \text{Var}[\text{Im}(r)] = \sigma_u^2 |s_i|^2 + \sigma_v^2 + \sigma_n^2 \equiv \sigma^2, \quad (8c)$$

where

$$\sigma_u^2 \equiv \text{Var} \left[\text{Re} \left(\sum_{g \neq g_d} \nu_g e^{j\theta_g} \right) \right] = \text{Var} \left[\text{Im} \left(\sum_{g \neq g_d} \nu_g e^{j\theta_g} \right) \right], \quad (8d)$$

$$\sigma_v^2 \equiv \text{Var} \left[\text{Re} \left(\sum_l v_l s_{(l)} \right) \right] = \text{Var} \left[\text{Im} \left(\sum_l v_l s_{(l)} \right) \right], \quad (8e)$$

$$\sigma_n^2 \equiv \text{Var} [\text{Re}(n)] = \text{Var} [\text{Im}(n)], \quad (8f)$$

$E[\cdot]$ is the expectation, $\text{Var}[\cdot]$ is the variance, and $\text{Re}(s_i)$ and $\text{Im}(s_i)$ are respectively the real and imaginary parts of s_i [31]. Therefore, $\text{Re}(r) \sim N(\rho \text{Re}(s_i), \sigma^2)$, and $\text{Im}(r) \sim N(\rho \text{Im}(s_i), \sigma^2)$, where $N(\mu, \sigma^2)$ is a Gaussian distribution with mean μ and variance σ^2 . Note that in (8e), we assume that the random variable v_l is stochastically equivalent for $l = 1, \dots, L$.

The distribution is scaled as $\sigma_u^2/\rho^2 = 1/\kappa$ using the Rician K-factor κ for the channel response u . The Rician K-factor for the channel response v_l is assumed to be zero. Then, the variable σ^2 in (8c) is rewritten as

$$\sigma^2 = \frac{\rho^2 |s_i|^2}{\kappa} + \sigma_v^2 + \sigma_n^2. \quad (9)$$

An important point is that the variance σ^2 is tuned as a function of the term σ_u^2 , which depends on the transmit power at the surrounding nodes. This indicates that the signals transmitted from the surrounding nodes (i.e., $\sum_{l=1}^L v_l s_{(l)}$) stochastically amplify the subthreshold symbol ρs_i to be detectable, which is explained by the SR phenomenon [30].

In (3), the received symbol r is fully described by two random variables, i.e., the amplitude a and phase ϕ . This means that the stochastic properties of the received symbol are characterized for a given s_i using the joint PDF of (a, ϕ) . Hence, making a change of variables, the joint PDF of the received symbol r is obtained as

$$p_{\sigma^2}(a, \phi|s_i) = N(\rho \text{Re}(s_i), \sigma^2) N(\rho \text{Im}(s_i), \sigma^2) |J|, \quad (10a)$$

where $|J|$ is the Jacobian matrix:

$$|J| = \begin{pmatrix} \frac{\partial(a \cos \phi)}{\partial a} & \frac{\partial(a \cos \phi)}{\partial \phi} \\ \frac{\partial(a \sin \phi)}{\partial a} & \frac{\partial(a \sin \phi)}{\partial \phi} \end{pmatrix}. \quad (10b)$$

B. Mutual Information

The mutual information is analyzed for a discrete memoryless channel between the source and the destination, as depicted in Fig. 3. The discrete memoryless channel is often used to discuss the detection performance and channel capacity [31]. For M input symbols $\{s_1, \dots, s_M\}$ transmitted from the source, the M output symbols $\{\hat{s}_1, \dots, \hat{s}_M\}$ detected at the destination are characterized with the transition probability

$$\begin{aligned} P_{ki} &\equiv P[\hat{s} = s_k | s_i] \\ &= \int_{\Omega_k} p_{\sigma^2}(a, \phi|s_i) da d\phi, \end{aligned} \quad (11)$$

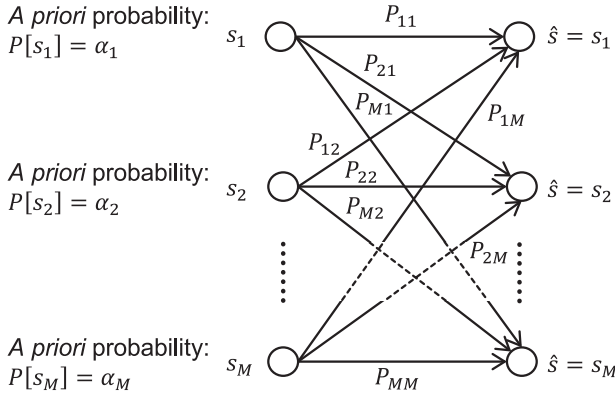


Fig. 3. Discrete memoryless channel used in the analysis of mutual information.

where $k = 1, 2, \dots, M$. The transmitted symbol is selected with a probability $P[s_i] \equiv \alpha_i$, i.e., the *a priori* probability. This transition probability is related to the signal transmitted from the surrounding nodes, $s_{(l)}$, because the transition probability P_{ki} is a function of the variance σ^2 .

When the sets of the transmitted and detected symbols are $S \equiv \{s_1, \dots, s_M\}$ and $\hat{S} \equiv \{\hat{s}_1, \dots, \hat{s}_M\}$, respectively, the mutual information is given as

$$I(S; \hat{S}) = \sum_{k=1}^M \sum_{i=1}^M P[s_i, \hat{s} = s_k] \log_2 \left(\frac{P[\hat{s} = s_k | s_i]}{P[\hat{s}_j = s_k]} \right). \quad (12)$$

Because $P[s_i, \hat{s} = s_k] = \alpha_i P[\hat{s} = s_k]$, $I(S; \hat{S})$ depends on the *a priori* probability α_i . Unfortunately, it is difficult to explicitly derive the mutual information because the channel transition probabilities in (11) are expressed as a double integral of two Gaussian functions. Therefore, our analysis should numerically calculate the mutual information.

C. Numerical Results

The analytical expression in (12) implies that the mutual information is dramatically enhanced owing to the presence of an interference symbol during weak signal reception. To clarify this point, we provide a numerical example of the mutual information regarding the variance σ_v^2 in Fig. 4. We encoded the transmitted symbols with equal probabilities: $\alpha_1 = \alpha_2 = \dots = \alpha_M = 1/M$. The parameters were set as $\rho|s_i| = 0.2$ and $\xi = 1$ to reflect the critical situation in which the received signal is not detectable at the destination (i.e., $\rho|s_i| \leq \xi$), as shown in Fig. 1(a). Clearly, when the interference symbol does not exist (i.e., $\sigma_v^2 = 0$, in other words, a conventional fading environment), the mutual information is zero. This means that no information is transferred from the source to the destination. In contrast, when $\sigma_v^2 > 0$, the mutual information takes a positive value. This demonstrates that the interference symbol helps to decode the weak symbol transmitted from the out-of-range source, which contributes to the enlargement of the communication range of the source. This point is analytically understandable from (3). In the presence of the interference symbol (i.e., the term $\sum_{l=1}^L v_l s_{(l)}$), the received

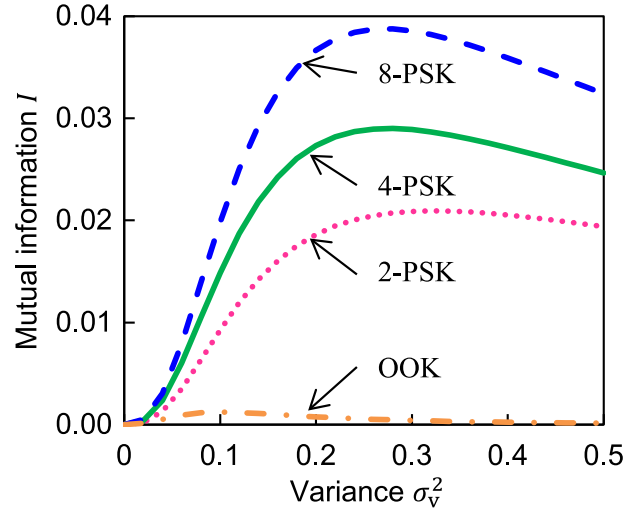


Fig. 4. Mutual information versus the variance σ_v^2 . The parameters are $\rho|s_i| = 0.2$, $\rho = 0.8$, $\kappa = 2$, $\sigma_n^2 = 0.01$, and $\xi = 1$.

symbol can exceed the detection limit even if the transmitted symbol is below the limit. The stochastic behavior of the interference symbols means that such an effect can be stochastically observed. In Section IV, the details of the mechanism are presented.

The results in Fig. 4 show interesting behavior; specifically, the mutual information is maximized at a certain value of the variance of the interference symbols. The mutual information is maximized at $\sigma_v^2 = 0.10, 0.32, 0.28$, and 0.27 , for OOK, 2-PSK, 4-PSK, and 8-PSK, respectively. This is a common feature of the proposed method regardless of the modulation scheme. It is noted that this maximization effect in terms of the variance is typical behavior in systems that exhibit SR [5]. A similar trend is also found in previous work focusing on the exploitation of interfering signals [30]. These results are evidence that our analyses are correct.

It is also noted that the fading environment needs to be identified for the proposed method. Channel estimation techniques, which have been thoroughly discussed in conventional wireless communications [36], should successfully enable channel identification for the proposed method.

IV. BEHAVIOR OF THE PROPOSED SYSTEM

A. Toy Model

The challenge described in this section is to identify the underlying signal detection mechanism of the proposed method. To reveal the contribution of the interference symbol, from (7), we introduce a *toy model* for the received symbol:

$$r = \rho s_i + v, \quad (13)$$

which describes the single path and noiseless channel between the source and the destination: $\sum_{g \neq g_d} v_g e^{j\theta_g} s_i = 0$ and $n = 0$. In addition, a single surrounding node is considered to provide the interference symbol: $L = 1$ and $v \equiv v_1 s_{(1)}$. This model allows us to explicitly derive the joint PDF of the received symbol

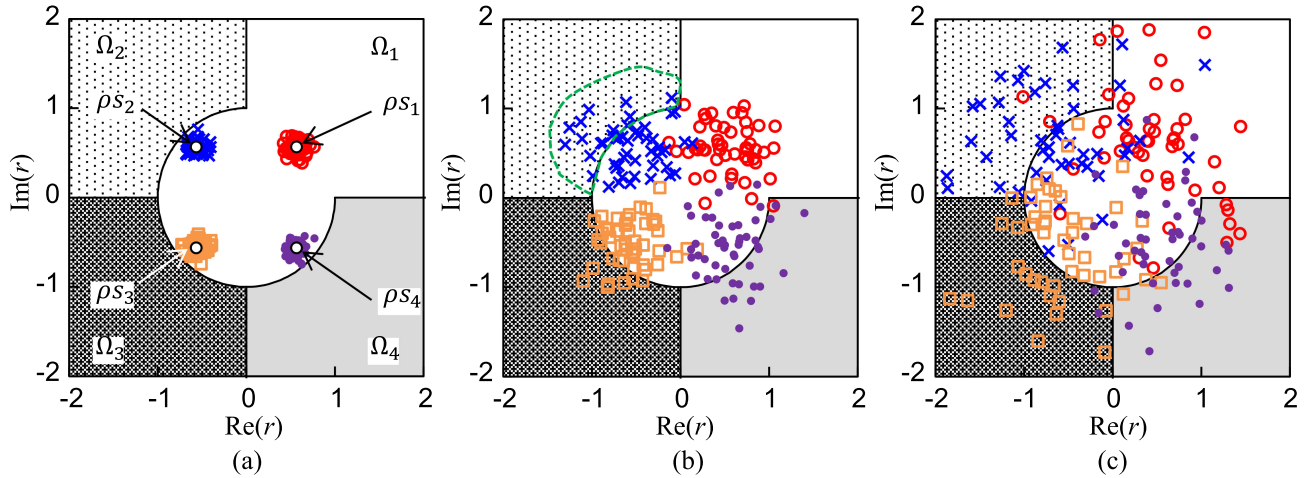


Fig. 5. Constellation diagrams of the received symbol r for 4-PSK at (a) $\sigma_v^2 = 0.005$, (b) $\sigma_v^2 = 0.09$, and (c) $\sigma_v^2 = 0.3$. The received symbols are plotted with circles, crosses, squares, and dots for $i = 1, 2, 3$, and 4 , respectively. The desired symbol strength and threshold level are $\rho|s_i| = 0.8$ and $\xi = 1$, respectively. Fifty constellation points for each message are sampled along with the probability in (14).

$p_{\sigma_v^2}(a, \phi|s_i)$, which is a key variable for signal enhancement based on the interference symbol.

Straightforwardly, the joint PDF in (10a) is now rewritten as

$$p_{\sigma_v^2}(a, \phi|s_i) = \frac{a}{2\pi\sigma_v^2} e^{-\frac{a^2 + \rho^2|s_i|^2 - 2\rho a|s_i|\cos(\phi - \arg(s_i))}{2\sigma_v^2}}, \quad (14)$$

where $\arg(\cdot)$ is the argument of a complex number. Equation (14) provides an important insight into the detectability of the subthreshold signal; the PDF varies in accordance with the variance σ_v^2 . Such a variation can be used for the detection of subthreshold symbols in the hard decision decoder in (5).

B. Enhancement Mechanism Exploiting the Interference Signal

Here, we discuss the detection mechanism of the proposed system using the derived PDF in (14) in the severe communication scenario where $\rho|s_i| \leq \xi$; that is, the transmitted symbol s_i is incorrectly estimated at the destination owing to the low strength of the received symbol. Such a scenario mostly occurs when the destination is outside the communication range of the source. Throughout the analysis presented here, we reveal that the interference symbol v amplifies the subthreshold signal ρs_i ; thus, the desired symbols s_i are successfully decoded at the destination.

Using 4-PSK as an example, we plot constellation diagrams of the received symbol r in Fig. 5. The strength of the desired symbol and the threshold level were $\rho|s_i| = 0.8$ and $\xi = 1$, respectively. Fifty constellation points were sampled for each message according to PDF in (14) for the variances $\sigma_v^2 = 0.005$, 0.09 , and 0.3 .

Note that, when $v = 0$, the constellation points of the received symbol are located at $r = 0.8 \exp(j(2i-1)\pi/4)$, as marked with the black circles, whose amplitude is less than the detection limit ξ . Therefore, the received symbol cannot be identified

at the destination when the surrounding nodes do not provide assistance.

In Fig. 5, the constellation points are scattered depending on σ_v^2 . For $\sigma_v^2 = 0.005$ in Fig. 5(a), all of the constellation points exist in region $\Omega_1 = \{(a, \phi) | a \leq \xi\}$. This means that the symbols are always detected as $\hat{s} = s_1$; that is, the received symbols cannot be identified at the destination. However, when the variance is increased to $\sigma_v^2 = 0.09$, some of the symbols emerge in the region $\{(a, \phi) | a > \xi\}$, as shown in Fig. 5(b). For example, the received symbols for ρs_2 (blue crosses) are partly found in region Ω_2 owing to the stochastic term v in (13) (these constellation points are enclosed by the green dashed circle). Hence, the transmitted symbol s_i is correctly, although slightly, identified at the destination. As σ_v^2 further increases, the received symbols spread over the undesired region $\Omega_{k \neq i}$. This wide scattering causes decision errors at the destination. For $\sigma_v^2 = 0.3$ in Fig. 5(c), for instance, the symbols of ρs_1 (red circles) are observed in regions Ω_2 and Ω_4 . This leads to erroneous detection because they actually belong in region Ω_1 .

To understand the statistical behavior in Fig. 5, we elucidate the probability of successful detection for s_2 in the following discussion. This probability is given as

$$\begin{aligned} P[r \in \Omega_2 | s_2] &= P[(a, \phi) \in \Omega_2 | s_2] \\ &= P[a > \xi | s_2] \cdot P[\pi/2 < \phi < \pi | s_2] \\ &= \int_{\xi}^{+\infty} p_{\sigma_v^2}(a | s_2) da \cdot \int_{\pi/2}^{\pi} p_{\sigma_v^2}(\phi | s_2) d\phi \\ &\equiv P_a(s_2) \cdot P_{\phi}(s_2) \end{aligned} \quad (15)$$

owing to the independence of a and ϕ . Moreover, $P_a(s_2)$ and $P_{\phi}(s_2)$ are the probabilities for which the amplitude of the received symbol exceeds the threshold ξ and the phase exists in $[\pi/2, \pi]$, respectively. The marginal PDFs included in (15)

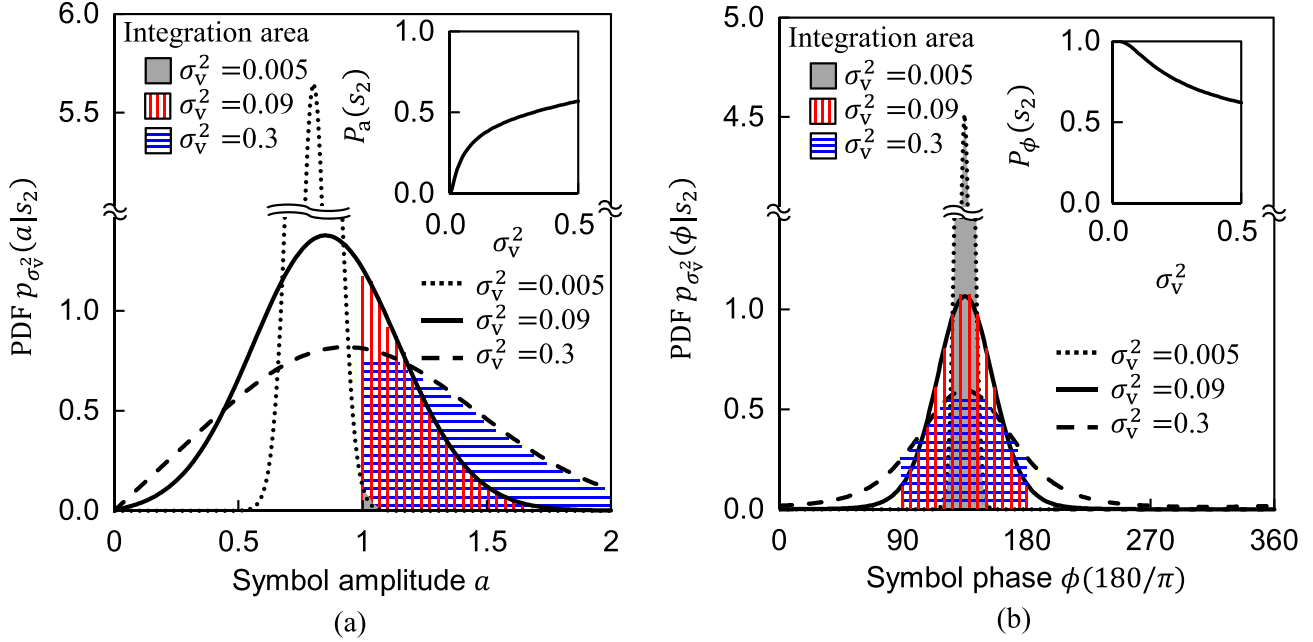


Fig. 6. Marginal PDFs of the symbol r : (a) amplitude $p_{\sigma^2}(a|s_2)$ and (b) phase $p_{\sigma^2}(\phi|s_2)$. The probabilities $P_a(s_2) = \int_{\xi}^{+\infty} p_{\sigma^2}(a|s_2)da$ and $P_\phi(s_2) = \int_{\pi/2}^{\pi} p_{\sigma^2}(\phi|s_2)d\phi$ are plotted in the insets of (a) and (b), respectively. The hatched regions are the ranges of integration used in the calculations of $P_a(s_2)$ and $P_\phi(s_2)$. The parameters used here are the same as those in Fig. 5.

are expressed as

$$\begin{aligned}
 & p_{\sigma_v^2}(a|s_i) \\
 &= \int_0^{2\pi} p_{\sigma_v^2}(a, \phi|s_i)d\phi = \frac{a}{\sigma_v^2} e^{-\frac{a^2 + \rho^2|s_i|^2}{2\sigma_v^2}} I_0\left(\frac{a\rho|s_i|}{\sigma_v^2}\right), \quad (16a) \\
 & p_{\sigma_v^2}(\phi|s_i) \\
 &= \int_0^{\infty} p_{\sigma_v^2}(a, \phi|s_i)da \\
 &= \frac{1}{2\pi} e^{-\frac{\rho^2|s_i|^2}{2\sigma_v^2}} \\
 &\cdot \left[1 + \sqrt{\frac{\pi}{2}} \frac{\rho|s_i| \cos(\phi - \arg(s_i))}{\sigma_v} e^{\frac{\rho^2|s_i|^2 \cos^2(\phi - \arg(s_i))}{2\sigma_v^2}} \right. \\
 &\quad \cdot \left. \left(1 + \operatorname{erf}\left(\frac{\rho|s_i| \cos(\phi - \arg(s_i))}{\sqrt{2}\sigma_v}\right) \right) \right], \quad (16b)
 \end{aligned}$$

where $I_0(\cdot)$ and $\operatorname{erf}(\cdot)$ denote the modified Bessel function of the first kind and the error function, respectively.

As addressed in [30], the detection limit can be effectively enhanced by exploiting interference signals in a statistical sense. To investigate such an effect in communication with an out-of-range node, Fig. 6(a) shows the marginal PDF of the amplitude, i.e., $p_{\sigma^2}(a|s_2)$, for several values of σ_v^2 . The parameters used here have the same values as those in Fig. 5. The hatched regions are the ranges of integration in the calculations of $P_a(s_2)$. At $\sigma_v^2 = 0.005$, the amplitude of the received symbols is mostly less than the threshold level $\xi = 1$, as plotted with the dotted curve. However, according to the increase in σ_v^2 , the PDF spreads

over the detectable region, $a > \xi$, as plotted with the solid and dashed curves at $\sigma_v^2 = 0.09$ and 0.3 , respectively. This means that the signal from the source node could often exceed the detection limit, which leads to correct detection. This effect is clearly observed in the inset of Fig. 6(a); the probability $P_a(s_2)$ is drastically enhanced with an increase in the variance σ_v^2 . Therefore, the concept described in [30] is also effective in the communication scenario with an out-of-range node.

In contrast to previous work [30], the phase—another important factor—should be considered in the discussion of the enhancement because this study focuses on the PSK modulation scheme. To discuss this point, Fig. 6(b) shows the marginal PDFs of the phase, i.e., $p_{\sigma^2}(\phi|s_2)$, for several values of σ_v^2 . The hatched regions are the ranges of integration in the calculations of $P_\phi(s_2)$. Unlike the symbol amplitude, an increase in the variance σ_v^2 has a negative effect on the phase ϕ . When the variance is small, e.g., $\sigma_v^2 = 0.005$, the phase is mostly located around $3\pi/4$, which is the original phase of the transmitted symbol s_2 . In this case, the interference symbol does not significantly affect symbol detection. When the variance σ_v^2 is large, such as $\sigma_v^2 = 0.09$ or 0.3 , the phase is distributed over a wide range of the phase space, thereby resulting in erroneous detection. This drawback is clearly observed in the inset of Fig. 6(b). Therefore, to communicate with an out-of-range node, interference signals that are too strong should be avoided.

As shown in Figs. 4 and 5, the variance σ_v^2 should be set to an adequate magnitude to obtain the most reliable detection. This interesting behavior is explained in terms of the inversely related probabilities $P_a(s_2)$ and $P_\phi(s_2)$. From (15), the probability of correct detection, $P[r \in \Omega_2|s_2]$, is written as

the product of $P_a(s_2)$ and $P_\phi(s_2)$. When the variance σ_v^2 is small (e.g., $\sigma_v^2 = 0.005$), $P[r \in \Omega_2 | s_2] \approx 0$ because $P_a(s_2) \approx 0$. This implies that the received symbols are incorrectly decoded. An incorrect decision is also made when the variance σ_v^2 is large (e.g., $\sigma_v^2 = 0.3$); this is because $P[r \in \Omega_2 | s_2]$ is degraded owing to the decrease in $P_\phi(s_2)$, which decreases faster than $P_a(s_2)$ increases. However, when σ_v^2 has an adequate magnitude (e.g., $\sigma_v^2 = 0.09$), the received symbol ρs_2 can partly reside in the desired region Ω_2 . This explanation is confirmed by the intuitive observation in Fig. 5.

V. PERFORMANCE LIMIT: CHANNEL CAPACITY

A. Channel Capacity

In this section, we discuss the channel capacity for the general propagation scenario presented in Section III to reveal the performance limit of the proposed method. The channel capacity is obtained via the maximization of the mutual information subject to the *a priori* probability α_i [31]. In addition, we require the interference level σ_v^2 to be optimized because the interference-aided enhancement strongly depends on the interference level [30]. Indeed, the term $P[\hat{s} = s_k | s_i]$ in (12) is a function of σ_v^2 . Thus, the channel capacity is obtained by solving the following optimization problem:

$$\max_{\alpha_1, \dots, \alpha_M, \sigma_v^2} I(S; \hat{S}) \quad \text{s.t.} \quad \sum_{i=1}^M \alpha_i = 1. \quad (17)$$

This problem should be solved with convex optimization algorithms, including the Nelder–Mead simplex method [37], even in a time-variant environment.

B. Numerical Results

Fig. 7 presents numerical examples of the channel capacity of the proposed method (solid curves), i.e., $\sigma_v^2 \neq 0$. These results were obtained by solving the problem in (17). For comparison, we also plotted the channel capacity without interference symbols (dotted curves), i.e., $\sigma_v^2 = 0$. The curves for both $\sigma_v^2 \neq 0$ and $\sigma_v^2 = 0$ increase according to the symbol strength $\rho |s_i|$, and they merge at $\rho |s_i| = 0.48, 0.81, 0.67,$ and 0.67 , for OOK, 2-PSK, 4-PSK, and 8-PSK, respectively. These points are highlighted with arrows in Fig. 7. In comparison with the curves for $\sigma_v^2 \neq 0$ and $\sigma_v^2 = 0$, the proposed method improves the channel capacity in the range of small amplitudes before they merge owing to the presence of the interference symbol. This contributes to the increased area coverage for the source.

For the problem in (17), there exist certain values of σ_v^2 and α_i that provide the greatest channel capacity. Such optimal values, which are denoted as $\check{\sigma}_v^2$ and $\check{\alpha}_i$, respectively, should depend on the strength of the symbol amplitude $\rho |s_i|$. To demonstrate this point, the optimal variance $\check{\sigma}_v^2$ is plotted in Fig. 8. The merge points shown in Fig. 7 are also marked in Fig. 8. A positive value of $\check{\sigma}_v^2$ is found at a lower symbol amplitude than that provided by the merge point. This means that the interference symbol enhances the channel capacity when the symbol amplitude is smaller than the merge point; that is, the received symbol is stochastically amplified by the interference symbol following

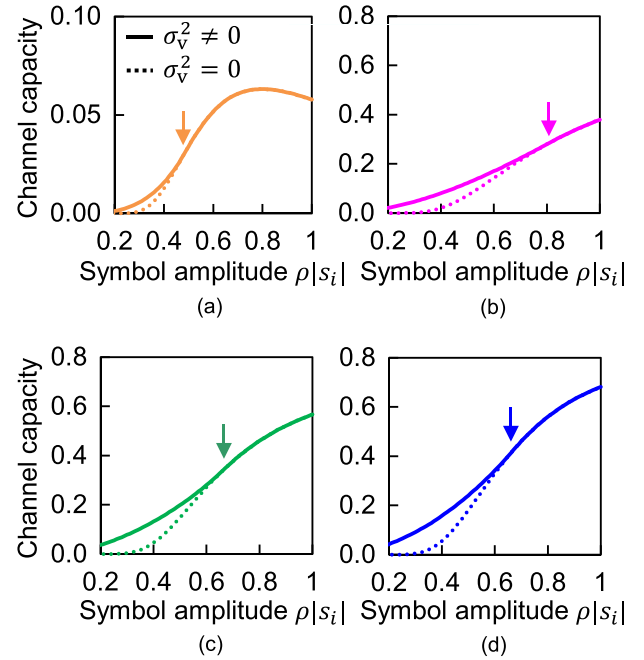


Fig. 7. Numerical examples of the channel capacity for (a) OOK, (b) 2-PSK, (c) 4-PSK, and (d) 8-PSK. Channel capacities with and without the interference symbol, $\sigma_v^2 \neq 0$ and $\sigma_v^2 = 0$, are plotted with solid and dotted curves, respectively. Both curves merge at the points indicated with arrows, where $\rho |s_i| = 0.48, 0.81, 0.67,$ and 0.67 for OOK, 2-PSK, 4-PSK, and 8-PSK, respectively. The parameters used here are $\rho = 0.8, \kappa = 2, \sigma_n^2 = 0.01,$ and $\xi = 1$.

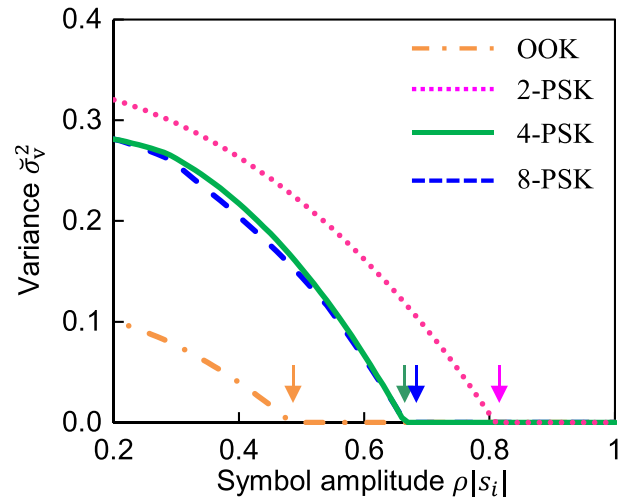


Fig. 8. Optimal variance $\check{\sigma}_v^2$ that gives the channel capacities shown in Fig. 7. The arrows indicate the merge points shown in Fig. 7. The parameters have the same values as those in Fig. 7.

the mechanism discussed in Section IV. Once the symbol amplitude reaches the merge point, the interference symbol is not required to obtain the channel capacity; that is, $\check{\sigma}_v^2 = 0$.

As with σ_v^2 , the *a priori* probability α_i should be optimized according to symbol amplitude $\rho |s_i|$ to obtain the channel capacity. Fig. 9 shows the optimal *a priori* probability $\check{\alpha}_i$ for the four modulation types studied here. The trends of the curves obviously change at the merge points. Interestingly, α_1 should

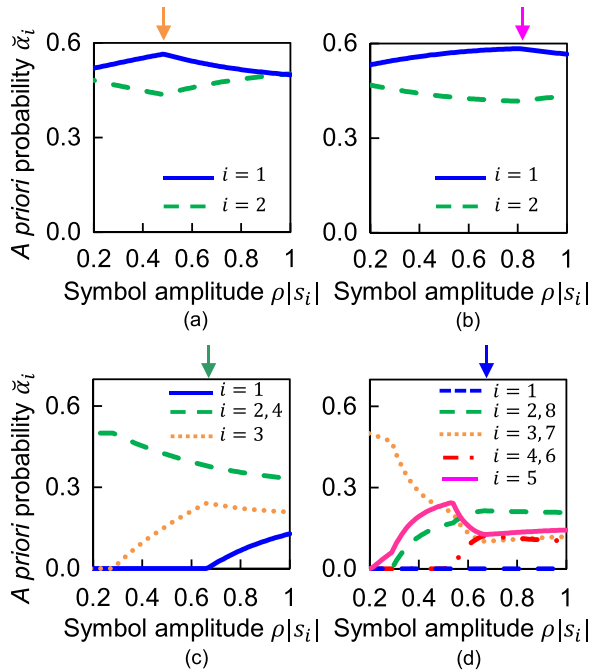


Fig. 9. Optimal *a priori* probabilities $\check{\alpha}_i$ for (a) OOK, (b) 2-PSK, (c) 4-PSK, and (d) 8-PSK modulation that give the channel capacity shown in Fig. 7. The arrows indicate the merge points shown in Fig. 7. The parameters have the same values as those in Fig. 7.

be coded as zero in the ranges where $0.20 \leq \rho|s_i| \leq 0.67$ for 4-PSK and $0.20 \leq \rho|s_i| \leq 1.00$ for 8-PSK. This indicates that, in these ranges, the symbol $s_{i=1}$ cannot carry any information. In this sense, the effective number of message points decreases to three for 4-PSK and seven for 8-PSK.

VI. CONCLUSION

We proposed a detection method that exploits interference signals to enhance radio coverage. In this method, a weak signal is stochastically amplified by utilizing the interference signals transmitted from the nodes around the destination. To evaluate the amplification effect, we calculated the mutual information. As a result, we showed that transmittable information increases in the presence of an interference signal. Moreover, a propagation toy model was introduced to explain the enhancement mechanism. The analysis using the toy model revealed that the optimal power of the interference signal maximizes the mutual information. In addition, we pointed out that the *a priori* probability of the transmitted symbols should be optimized to obtain the channel capacity.

Successful symbol detection at the destination node verified that the proposed method offers a direct wireless link to out-of-range nodes. Therefore, the proposed method could be an important building block for future communication applications such as device-to-device and Internet of Things networks.

ACKNOWLEDGMENT

The authors would like to thank Mr. Yasuo Nakashima for fruitful discussions.

REFERENCES

- [1] B. Zhou, H. Hu, S.-Q. Huang, and H.-H. Chen, "Intracluster device-to-device relay algorithm with optimal resource utilization," *IEEE Trans. Veh. Technol.*, vol. 62, no. 5, pp. 2315–2326, Jun. 2013.
- [2] Z. Yang, Z. Ding, P. Fan, and G. K. Karagiannidis, "Outage performance of cognitive relay networks with wireless information and power transfer," *IEEE Trans. Veh. Technol.*, vol. 65, no. 5, pp. 3828–3833, May 2016.
- [3] J. H. Winters, J. Salz, and R. Gitlin, "The impact of antenna diversity on the capacity of wireless communication systems," *IEEE Trans. Commun.*, vol. 42, no. 234, pp. 1740–1751, Feb./Mar./Apr. 1994.
- [4] R. Benzi, A. Sutera, and A. Vulpiani, "The mechanism of stochastic resonance," *J. Phys. A, Math. Gen.*, vol. 14, pp. L453–L457, 1981.
- [5] L. Gammaitoni, P. Hänggi, P. Jung, and F. Marchesoni, "Stochastic resonance," *Rev. Mod. Phys.*, vol. 70, pp. 223–287, Jan. 1998.
- [6] J. K. Douglass, L. Wilkens, E. Pantazelou, and F. Moss, "Noise enhancement of information transfer in crayfish mechanoreceptors by stochastic resonance," *Nature*, vol. 365, no. 6444, pp. 337–340, Sep. 1993.
- [7] S. Fauve and F. Heslot, "Stochastic resonance in a bistable system," *Phys. Lett. A*, vol. 97, no. 1, pp. 5–7, Aug. 1983.
- [8] P. Hänggi, "Stochastic resonance in biology. How noise can enhance detection of weak signals and help improve biological information processing," *ChemPhysChem*, vol. 3, no. 3, pp. 285–290, Mar. 2002.
- [9] A. Longtin, "Stochastic resonance in neuron models," *J. Stat. Phys.*, vol. 70, no. 1, pp. 309–327, Jan. 1993.
- [10] M. D. McDonnell and D. Abbott, "What is stochastic resonance? Definitions, misconceptions, debates, and its relevance to biology," *PLoS Comput. Biol.*, vol. 5, no. 5, May 2009, Art no. e1000348.
- [11] K. Wiesenfeld and F. Moss, "Stochastic resonance and the benefits of noise: from ice ages to crayfish and SQUIDS," *Nature*, vol. 373, no. 6509, pp. 33–36, Jan. 1995.
- [12] A. Ichiki and Y. Tadokoro, "Relation between optimal nonlinearity and non-Gaussian noise: Enhancing a weak signal in a nonlinear system," *Phys. Rev. E*, vol. 87, no. 1, Jan. 2013, Art no. 012124.
- [13] H. A. Braun, H. Wissing, K. Schäfer, and M. C. Hirsch, "Oscillation and noise determine signal transduction in shark multimodal sensory cells," *Nature*, vol. 367, no. 6460, pp. 270–273, Jan. 1994.
- [14] J. J. Collins, C. C. Chow, and T. T. Imhoff, "Stochastic resonance without tuning," *Nature*, vol. 376, pp. 236–238, Jul. 1995.
- [15] M. Kocaoglu, B. Gulbahar, and O. Akan, "Stochastic resonance in Graphene bilayer optical nanoreceivers," *IEEE Trans. Nanotechnol.*, vol. 13, no. 6, pp. 1107–1117, Nov. 2014.
- [16] B. McNamara, K. Wiesenfeld, and R. Roy, "Observation of stochastic resonance in a ring laser," *Phys. Rev. Lett.*, vol. 60, pp. 2626–2629, Jun. 1988.
- [17] E. Simonotto, M. Riani, C. Seife, M. Roberts, J. Twitty, and F. Moss, "Visual perception of stochastic resonance," *Phys. Rev. Lett.*, vol. 78, pp. 1186–1189, Feb. 1997.
- [18] H. Chen, L. R. Varshney, and P. K. Varshney, "Noise-enhanced information systems," *Proc. IEEE*, vol. 102, no. 10, pp. 1607–1621, Oct. 2014.
- [19] Y. Tadokoro, S. Kasai, A. Ichiki, and H. Tanaka, "Design framework of image sensor system based on the effect of supra-threshold stochastic resonance," *IEEE Trans. Syst., Man, Cybern., Syst.*, vol. 46, no. 8, pp. 1121–1128, Aug. 2016.
- [20] S. Mitaim and B. Kosko, "Adaptive stochastic resonance in noisy neurons based on mutual information," *IEEE Trans. Neural Netw.*, vol. 15, no. 6, pp. 1526–1540, Nov. 2004.
- [21] A. Patel and B. Kosko, "Stochastic resonance in continuous and spiking neuron models with levy noise," *IEEE Trans. Neural Netw.*, vol. 19, no. 12, pp. 1993–2008, Dec. 2008.
- [22] J. Teramae and T. Fukai, "Computational implications of lognormally distributed synaptic weights," *Proc. IEEE*, vol. 102, no. 4, pp. 500–512, Apr. 2014.
- [23] D. He, "Chaotic stochastic resonance energy detection fusion used in cooperative spectrum sensing," *IEEE Trans. Veh. Technol.*, vol. 62, no. 2, pp. 620–627, Feb. 2013.
- [24] Q. Li and Z. Li, "A novel sequential spectrum sensing method in cognitive radio using suprathreshold stochastic resonance," *IEEE Trans. Veh. Technol.*, vol. 63, no. 4, pp. 1717–1725, May 2014.
- [25] J. Wang, X. Ren, S. Zhang, D. Zhang, H. Li, and S. Li, "Adaptive bistable stochastic resonance aided spectrum sensing," *IEEE Trans. Wireless Commun.*, vol. 13, no. 7, pp. 4014–4024, Jul. 2014.
- [26] D. He, Y. Lin, C. He, and L. Jiang, "A novel spectrum-sensing technique in cognitive radio based on stochastic resonance," *IEEE Trans. Veh. Technol.*, vol. 59, no. 4, pp. 1680–1688, May 2010.

- [27] J. Liu, Z. Li, L. Guan, and L. Pan, "A novel parameter-tuned stochastic resonator for binary PAM signal processing at low SNR," *IEEE Commun. Lett.*, vol. 18, no. 3, pp. 427–430, Mar. 2014.
- [28] Y. Nakashima, T. Yamazato, S. Arai, H. Tanaka, and Y. Tadokoro, "Noise-aided demodulation with one-bit comparator for multilevel pulse-amplitude-modulated signals," *IEEE Wireless Commun. Lett.*, vol. 7, no. 5, pp. 848–851, Oct. 2018.
- [29] S. Kay, "Can detectability be improved by adding noise?" *IEEE Signal Process. Lett.*, vol. 7, no. 1, pp. 8–10, Jan. 2000.
- [30] S. Hiraoka, Y. Nakashima, T. Yamazato, S. Arai, Y. Tadokoro, and H. Tanaka, "Interference-aided detection of subthreshold signal using beam control in polarization diversity reception," *IEEE Commun. Lett.*, vol. 22, no. 9, pp. 1926–1929, Sep. 2018.
- [31] J. G. Proakis, *Digital Communications*. New York, NY, USA: McGraw-Hill, 2001.
- [32] K. N. Le, "Distributions of even-degree-of-freedom generalised-Rician fading for opportunistic-relay selection employing MRC under outdated-CSI conditions," *IEEE Trans. Commun.*, vol. 67, no. 9, pp. 6441–6455, Sep. 2019.
- [33] K. N. Le, "Opportunistic outdated relays under even-degree-of-freedom generalized-rician fading," *IEEE Trans. Veh. Technol.*, vol. 68, no. 3, pp. 2472–2487, Mar. 2019.
- [34] M. Jaber, F. J. Lopez-Martinez, M. A. Imran, A. Sutton, A. Tukmanov, and R. Tafazolli, "Wireless backhaul: Performance modeling and impact on user association for 5G," *IEEE Trans. Wirel. Commun.*, vol. 17, no. 5, pp. 3095–3110, May 2018.
- [35] B. Domazetovi and E. Koan, "Packet error rate in IEEE 802.11ah use case scenarios," in *Proc. 25th Telecommun. Forum*, Nov. 21–22, 2017, pp. 1–4.
- [36] J.-J. V. de Beek, O. Edfors, M. Sandell, S. K. Wilson, and P. O. Borjesson, "On channel estimation in OFDM systems," in *Proc. 45th Veh. Technol. Conf.*, vol. 2, Aug. 1995, pp. 815–819.
- [37] J. C. Lagarias, J. A. Reeds, M. H. Wright, and P. E. Wright, "Convergence properties of the Nelder-Mead simplex method in low dimensions," *SIAM J. Optim.*, vol. 9, pp. 112–147, Jul. 1998.



Hiroya Tanaka (M'05–SM'17) received the B.E. degree from Saitama University, Saitama, Japan, in 2003, and the M.E. and D.E. degrees from the Tokyo Institute of Technology, Tokyo, Japan, in 2005 and 2008, respectively. Since 2008, he has been with the Toyota Central Research and Development Laboratories Inc. His current interests are nanostructured electromagnetic devices, nonlinear circuit elements, and applied radio instrumentation and measurements.



Shintaro Hiraoka (S'17) received the B.S. degree in electrical and electronics engineering from Mie University, Japan, in 2017 and the M.S. degree in information and communication engineering from Nagoya University, Japan, in 2019. Since 2019, he has been with the Chūkyō Television Broadcasting Co., Ltd. His research interests include stochastic resonance. He is a Student Member of the IEICE.



Takaya Yamazato (S'91–M'93–SM'16) received the Ph.D. degree from Keio University, Yokohama, Japan, in 1993. He is currently a Professor with the Institute of Liberal Arts and Sciences, Nagoya University, Japan. His research interests include visible light communication, ITS, and e-learning. In 1998, he gave a half-day tutorial entitled "Introduction to CDMA ALOHA" at the IEEE Globecom held in Sydney, Australia. In 2006, he received the IEEE Communication Society's Best Tutorial Paper Award.

He served as the Co-Chair of the Wireless Communication Symposia of the IEEE ICC 2009. He was the Co-Chair of Selected Areas in Communication Symposia of the IEEE ICC 2011. From 2008 to 2010, he served as the Chair of the Satellite and Space Communication Technical Committee of the IEEE Communication Society. In 2011, he gave a half-day tutorial entitled "Visible Light Communication" at the IEEE ICC 2011 held in Kyoto, Japan. From 2017 to 2018, he was the Director of Asia/Pacific Board, the IEEE Communication Society. He served as the Editor-in-Chief for the Japanese Section of the *IEICE Transactions on Communications* from 2009 to 2011.



Shintaro Arai (S'06–M'09) received the B.E., M.E., and D.E. degrees from Tokushima University, Tokushima, Japan, in 2004, 2006 and 2009, respectively. From January 2007 to December 2008, he was a Special Research Student with Nagoya University, Japan. From April 2009 to March 2011, he worked as a Postdoctoral Fellow with the ITS Laboratory, Aichi University of Technology, Japan. From April 2011 to March 2016, he worked as a Research Associate with the National Institute of Technology, Kagawa College, Japan. Since April 2016, he has been a Lecturer

with the Okayama University of Science, Japan. His research interests include visible light communication systems, chaos-based communication systems, and stochastic resonance phenomena. He is a Member of the IEICE.



Yukihiro Tadokoro (M'00–SM'18) received the B.E., M.E., and Ph.D. degrees in information electronics engineering from Nagoya University, Aichi, Japan, in 2000, 2002, and 2005, respectively. Since 2006, he has been with the Toyota Central Research and Development Laboratories., Inc. He was a Research Scholar with the Department of Physics and Astronomy, Michigan State University, East Lansing, MI, USA, in 2011 and 2012, to study nonlinear phenomena for future applications in signal and information processing fields. Since 2019, he has been a

Visiting Professor with the Graduate School of Informatics, Nagoya University. His current research interests include nanoscale wireless communication, noise-related phenomena in nonlinear systems, and their applications in vehicles and nanoscale systems. Dr. Tadokoro is a Senior Member of the Institute of Electronic, Information and Communication Engineers, Japan.